Cell Motility and the Cytoskeleton 37:363–377 (1997)

Distribution and Orientation of Rhodamine-Phalloidin Bound to Thin Filaments in Skeletal and Cardiac Myofibrils

Vladimir Zhukarev,[1] Jean M. Sanger,[2] Joseph W. Sanger,[2] Yale E. Goldman,[1] and Henry Shuman[1]*

[1]*Department of Physiology, Pennsylvania Muscle Institute, University of Pennsylvania School of Medicine, Philadelphia*
[2]*Department of Cell and Developmental Biology, Pennsylvania Muscle Institute, University of Pennsylvania School of Medicine, Philadelphia*

Phalloidin staining of muscle does not reflect the known disposition of sarcomeric thin filaments. Quantitative image analysis and steady-state fluorescence polarization microscopy are used to measure the local intensity and orientation of tetramethyl rhodamine-labeled phalloidin (TR-phalloidin) in skinned myofibrils. TR-phalloidin staining of isolated skeletal myofibrils labeled while in rigor reveals fluorescence that is brighter at the pointed ends of the thin filaments and Z lines than it is in the middle of the filaments. In cardiac myofibrils, phalloidin staining is uniform along the lengths of the thin filaments in both relaxed and rigor myofibrils, except in 0.2-μm dark areas on either side of the Z line. Extraction of myosin or tropomyosin-troponin molecules does not change the nonuniform staining. To test whether long-term storage in glycerol changes the binding of phalloidin to thin filaments in myofibrils, minimally permeabilized (briefly skinned) myofibrils, or myofibrils stored in glycerol for at least 7 days (glycerol extraction) were compared. TR-phalloidin was well ordered throughout the sarcomere in briefly skinned skeletal and cardiac myofibrils, but TR-phalloidin bound to the Z line and pointed ends of thin filaments was randomly oriented in glycerol-extracted myofibrils, suggesting that the ends of the thin filaments become disordered after glycerol extraction. In relaxed skeletal myofibrils with sarcomere lengths greater than 3.0 μm, staining was nearly uniform all along the actin filaments. Exogenous bare actin filaments polymerized from the Z line (Sanger et al., 1984: *J. Cell Biol.* 98:825–833) in and along the myofibril bind rhodamine phalloidin uniformly. Our results support the hypothesis that nebulin can block the binding of phalloidin to actin in skeletal myofibrils and nebulette can block phalloidin binding to cardiac thin filaments. Cell Motil. Cytoskeleton 37:363–377, 1997.

Key words: actin; myosin; titin; nebulin; fluorescence polarization; muscle

INTRODUCTION

Phalloidin is a cyclic heptapeptide from the mushroom *Amanita phalloides* that binds to filamentous actin with nanomolar affinity and stabilizes the filaments against depolymerization [Wehland et al., 1977]. These properties are apparently due to the interaction of each phalloidin molecule with three adjacent actin monomers in F-actin [Lorenz et al., 1993]. Labeled with fluorescent probes, phalloidin is used widely to localize actin fila-

Contract grant sponsor: NIH; Contract grant numbers: HL-15835, HL-48954; Contract grant sponsor: NSF; Contract grant number: MCB-93-19041.

*Correspondence to: Henry Shuman, Department of Physiology, Pennsylvania Muscle Institute, University of Pennsylvania School of Medicine, Philadelphia, PA 19104.

Received 6 February 1997; accepted 26 March 1997.

ments in fixed cells [see review by Faulstich et al., 1988] and in many in vitro assays of myosin-based motility. Fluorescent derivatives of phalloidin can also be used to provide quantitative information about the orientation of actin filaments. When tetramethyl rhodamine-phalloidin was bound to F-actin, the fluorescence emission transition moment of the probe was estimated by fluorescence polarization to be oriented at 31° relative to the filament axis [Kinosita et al., 1991]. Based on this axial orientation, fluorescent probes attached to phalloidin have been used to measure the orientation of sarcomeric actin in glycerinated muscle fibers during contractions [Prochniewicz-Nakayama et al., 1983] and in cell motility assays during filament sliding [Kinosita et al., 1991]. Similar measurements have been made in fixed cells to determine the orientation of actin filaments in intestinal microvilli [Borejdo and Burlacu, 1993], in the cleavage furrows of dividing cells [Fishkind and Wang, 1993], and in the tails of filaments nucleated by *Listeria monocytogenes* [Zhukarev et al., 1995].

It is often assumed that phalloidin staining identifies all filamentous actin in fixed or permeabilized cells. However, there have been several reports that phalloidin sometimes fails to bind to all of the F-actin in muscle myofibrils. Phalloidin does not bind uniformly along the actin filaments in isolated skeletal muscle myofibrils [Bukatina et al., 1984; Wilson et al., 1987; Szczesna and Lehrer, 1993; Ao and Lehrer, 1995]. It is bright at the Z bands and at the pointed ends of the thin filaments and has been described as either absent or nonuniform in the middle regions of the thin filaments. The high level of staining in the Z bands has been attributed to overlap of actin filaments from adjacent sarcomeres at the Z bands [Ao and Lehrer, 1995]. The reduction of staining in the middle of the filaments could be due to steric hindrance by nebulin covering the phalloidin binding sites [Ao and Lehrer, 1995]. Prolongation of the period of storage or staining of the myofibrils enhances phalloidin binding, presumably by extracting or competing with sarcomeric components that block the phalloidin binding sites. Cardiac myofibrils, which lack nebulin [Locher and Wild, 1986] but contain a truncated form called nebulette [Moncman and Wang, 1995], were reported to stain uniformly with phalloidin along the entire length of the thin filaments [Ao and Lehrer, 1995].

The present study was undertaken to determine the characteristics and cause of the nonuniform phalloidin staining of isolated cardiac and skeletal myofibrils. The staining pattern at various sarcomere lengths helped identify the structural components responsible for the regions of phalloidin binding within the myofibril. We used fluorescence polarization microscopy to test whether the orientation of phalloidin in the various bands is consistent with specific binding to normally oriented actin filaments in those locations. Because other myofibrillar proteins, such as myosin or tropomyosin, might also interfere with phalloidin binding, we tested staining in conditions which extract these proteins or modify their interaction with actin, and we tested staining to pure actin filaments newly polymerized within or around myofibrils.

The present study supports the previous suggestion that nebulin may interfere with the binding of phalloidin to the thin filaments [Ao and Lehrer, 1995], but we also have detected a region of reduced staining in cardiac myofibrils that may indicate the effect of nebulette. Phalloidin bound in the Z lines and tips of thin filaments in myofibrils exposed to glycerol for several weeks is disordered, suggesting that the actin in these regions becomes disordered or that phalloidin binds to other sarcomeric components. Some of the results have been presented in abstract form [Zhukarev et al., 1995, 1996a,b].

MATERIALS AND METHODS

Chemicals and Preparation of Proteins

Phalloidin-tetramethyl rhodamine isothiocyanate conjugate was obtained from Fluka Chemical Corporation (Ronkonkoma, NY). Unlabeled phalloidin was purchased from Sigma Corporation (St. Louis, MO). α-Actinin, actin, and bovine serum albumin (BSA) were prepared and fluorescently labeled as previously described [Sanger et al., 1984; Danowski et al., 1992]. All organic and inorganic chemicals used in this study were of the highest grade (Fisher Scientific Co., Pittsburgh, PA).

Preparation of Myofibrils

Rabbit psoas muscle bundles were prepared in two ways: (a) short-term (i.e., overnight) skinning and (b) long-term (>7 days) glycerination. These two preparations are called briefly skinned and glycerol extracted, respectively, in the remainder of the article. For brief skinning, freshly dissected muscle bundles mounted on sticks were immersed in skinning solution at 4°C: 170 mM potassium propionate (KP), 5 mM ethyleneglycol-*bis*-(β-aminoethylether)-*N*,*N*,*N′*,*N′*-tetraacetic acid (EGTA), 2.5 mM $MgCl_2$, 10 mM imidazole, 2.5 mM ATP, 0.2 mM phenylmethylsulphonyl fluoride (PMSF), pH 7.0. For long-term glycerination, muscle bundles mounted on sticks were immersed in glycerination solution at −20°C: 170 mM KP, 5 mM EGTA, 2.5 mM $MgCl_2$, 10 mM imidazole, 2.5 mM ATP, 1 mM NaH_3, 50% glycerol, pH 7.0. [Goldman et al., 1984]. Rabbit cardiac bundles were prepared the same as the briefly skinned skeletal muscle bundles.

Rabbit psoas and cardiac myofibrils were prepared from skinned muscle bundles by homogenization (Sorvall Omni-Mixer, DuPont Instruments, Chadds Ford, PA) in Mg-rigor solution kept at 4°C with no detergent added:

100 mM N-tris[hydroxymethyl]methyl-2-aminoethanesulphonic acid (TES), 53 mM EGTA, 3 mM $MgCl_2$, pH 7.1.

Suspensions of myofibrils were deposited in 35-mm glass-bottom microwell dishes (MatTek, Ashland, MA) while in rigor solution and allowed to adhere for 15 min. The myofibrils were labeled while kept on ice with 0.5–1 μM rhodamine-phalloidin for short (30 min) or long (3–12 h) times. The results for long- and short-term labeling of fibrils with phalloidin were the same, and only the data for short-term labeling are presented. For several experiments, after the myofibrils were attached but before phalloidin labeling, the Mg-rigor solution was replaced with 15 mM ATP relaxing solution: 100 mM TES, 15 mM NaATP, 10 mM EGTA, 15.3 mM $MgCl_2$, 10 mM glutathione, 18.2 mM 1,6-diaminohexane-*N,N,N′,N′*,-tetraacetic acid (HDTA), pH 7.1.

Fluorescence Polarization Measurements

Fluorescence was measured with the myofibrils in either rigor or relaxing solution to match the solution used for phalloidin labeling. Fluorescence was always measured in solutions containing an oxygen scavenger system (composed of glucose, glucose-oxydase, and catalase), as described by Kishino and Yanagida [1988]. As an additional precaution, to prevent diffusion of oxygen to the myofibrils, the myofibrils and solutions were kept under a 2-mm layer of paraffin oil.

Fluorescence polarization microscopy and image processing were done essentially as described by Zhukarev et al. [1995]. A Nikon Diaphot inverted microscope was modified with sliders on both the excitation and emission ports. Each slider contained two linear polarizers (Melles Griot, Irvine, CA), one vertical and the other horizontal. A cooled CCD camera (Photometrics, Tuscon, AZ) was controlled by Image-1 software (Universal Imaging Corp., West Chester, PA) to acquire four different fluorescence polarization images: $\|I_\perp$, $_\perp I_\perp$, $\|I_\|$, $_\perp I_\|$, where the first subscript is the excitation and the second is the emission polarization direction parallel ($\|$) or perpindicular ($\perp$) to the cylindrical symmetry axis of the myofibril. To compensate for photobleaching, the four different fluorescence polarization images were taken in duplicate in the following order: $\|I_\perp$, $_\perp I_\perp$, $\|I_\|$, $_\perp I_\|$, $_\perp I_\|$, $\|I_\|$, $_\perp I_\perp$, $\|I_\perp$. For analysis, images were transferred to an Iris workstation (Silicon Graphics, Mountain View, CA) and processed with Semper software (Synoptics, Cambridge, UK). The sets of images were aligned to better than a fraction of a pixel, thereby correcting for image shifts introduced when changing the emission polarizers, by using the cross-correlation routines available in the Semper package. After alignment of the images, corresponding duplicate pairs of images were averaged. Slides of epoxy-embedded rhodamine were used to measure systematic polarization introduced by the microscope components [Axelrod, 1979], primarily due to the dichroic mirror, and polarized fluorescence intensities were corrected for these errors. The depolarization introduced by the high NA objective lens was considerable but was left uncorrected, and relative polarizations compared. Two polarization ratios were computed at each pixel in the images:

$$P_\| = (\|I_\| - \|I_\perp)/(\|I_\| + \|I_\perp)$$

$$\text{and } P_\perp = (_\perp I_\perp - _\perp I_\|)/(_\perp I_\perp + _\perp I_\|)$$

For pixels where the denominator is close to zero, such as background, noise in the images can give rise to large artifactual polarization ratios. Average ratios were computed from regions of the images where the fluorescence intensities were substantially higher than the background fluorescence. To suppress the background noise in images of polarization ratios, a two-dimensional color coding scheme was developed (see below). The ''total fluorescence images'' were computed from the sum of the individual polarization images: total fluorescence = $\|I_\| + 2\ _\perp I_\| + 8/3\ _\perp I_\perp + 2\ \|I_\perp$ [Allen et al., 1996]; (Dale et al., in preparation).

Maximum Entropy and Wiener Deconvolution

To deconvolve the point spread function from the total fluorescence image, we used a fast-Fourier-transform-based optimal Wiener filter [Press et al., 1988] or the maximum entropy method [Kuzuo and Tanaka, 1993] (for details, see the Appendix). In either case, the deconvolution was performed on a one- rather than two-dimensional data set. A model point spread function (psf) was estimated from the intensity profile of a single actin filament. The model psf was then used to deconvolve a one-dimensional sarcomere intensity profile obtained by projecting the intensities of a fibril image onto its long axis. The resultant deconvolved images by using the Wiener filter contained more ripples than those obtained by using the maximum entropy method.

Two-Dimensional Color Coding

To show both the polarization ratio and fluorescence intensity data in single images, data were digitally transformed so that the total fluorescent intensity of the object was stored in the least significant 4 bits and the polarization ratio in the most significant 4 bits at each pixel of an 8-bit binary image. The transformed images were displayed with Publisher's Paintbrush software (Zsoft Inc., Atlanta, GA) as pseudo-color images by using the color palettes shown in Figures 7, 8, and 10. The palettes consisted of 16 different hues ranging from red to violet, with each hue having 16 different intensities,

similar to that used by Tsien and Harootunian [1990] for calcium images. The polarization ratio at each pixel was coded as a hue, with red assigned to the highest ratio in the image and violet to the lowest ratio. Pixels with intermediate ratios were linearly transformed to 1 of the remaining 14 hues. The intensity of each displayed pseudocolor pixel was scaled to the intensity of the corresponding pixel in the total fluorescence image.

Extractions

Myofibrils were extracted with a high salt solution (0.6 M KCl, 10 mM Na pyrophosphate, 0.1 M KH_2PO_4, 1 mM $MgCl_2$, pH 6.4, 4°C) for 15 min to remove the myosin and the tropomyosin–troponin complex. The tropomyosin–troponin complex was removed from isolated myofibrils separately from myosin during an 1-h extraction in 1 mM sodium bicarbonate, pH 8.0, solution at 4°C [Sanger et al., 1984]. The myofibrils were rinsed several times with the bicarbonate solution and then several more times with low salt wash (0.1 M KCl, 10 mM phosphate buffer, 1 mM $MgCl_2$, pH 7.0).

Actin Polymerized Within Myofibrils

New, bare actin filaments were induced to form in and along isolated skeletal myofibrils in two different ways [Sanger et al., 1984]. In both procedures, myofibrils attached to coverslips were exposed to unlabeled phalloidin for 1 h to bind all of the available endogenous myofibril actin molecules. In one of the procedures, unlabeled α-actinin was added with the unlabeled phalloidin. The excess α-actinin and unlabeled phalloidin were removed with several rinses of the low salt solution. Monomeric actin was added to the myofibrils under polymerizing conditions, as previously described [Sanger et al., 1984]. After 30 min, the unbound actin was removed by several rinses of the low salt wash. The myofibrils were then exposed to rhodamine phalloidin for 1 h, rinsed with the low salt wash, and then examined in the microscope.

This procedure was also repeated without the addition of α-actinin to the myofibrils.

RESULTS

Sarcomeric Distibution of Phalloidin Binding

The thin filaments of glycerinated skeletal muscle do not stain uniformly with the fluorescent probe tetramethyl rhodamine-phalloidin (TR-phalloidin) [Bukatina et al., 1984; Szczesna and Lehrer, 1993], whereas actin filaments formed from purified monomeric actin molecules stain uniformly with phalloidin [Kinoshita et al., 1991; Zhukarev et al., 1995]. To determine whether protein extraction during glycerination alters TR-phalloidin binding, two groups of skinned myofibrils from skeletal muscle were prepared for labeling. In the first group, bundles of rabbit psoas muscle were briefly skinned for 16–18 h, and in the second, bundles were glycerol extracted for at least 7 days, during which partial extraction of nebulin and titin is expected to occur [Larsson and Moss, 1993; Wang, 1984]. Both briefly skinned and glycerol-extracted fibers were labeled for 30 min at 4°C and analyzed while in rigor. The fluorescence intensity distribution in the sarcomere is nearly the same for the two groups of myofibrils (Fig. 1). The pattern contained three distinct regions: a narrow bright band at the Z line (arrow, Fig. 1A,C), one or two bright bands (depending on sarcomere length) that flanked the H zone and appear to correspond to the pointed ends of the thin filaments (arrowheads, Fig. 1A,C), and lower fluorescence intensity regions between the Z line and the bands flanking the H zone. Myofibrils stained with TR-phalloidin for 12 h had the same fluorescence intensity distribution.

To measure the fluorescence intensity in the three distinct bands, the spatial resolution of the images was numerically enhanced. The fluorescence intensity distribution from muscle fibers is broadened by the psf of the microscope. The broadening of the bright bands of fluorescence from the Z line and bands flanking the H zone influences accurate measurements of the intensity in the middle portion of the thin filament. To minimize the intensity overlap between adjacent bands the resolution of one-dimensional intensity, profiles (Fig. 2A) were improved by using a Wiener filter (Fig. 2B) or maximum entropy deconvolution (Fig. 2C). The intensity profiles deconvolved with the maximum entropy method had fewer ripples than those obtained with the Wiener filter method. The percentage of total fluorescence in each region of the sarcomere, after deconvolution with the maximum entropy method, is shown in Table I. More than 70% of the total phalloidin bound to skeletal myofibrils is bound at the Z line or in the bands flanking the H zone.

To determine whether the rigor cross bridges affected phalloidin binding, myofibrils were labeled and measured while in relaxing solution after they had been prepared and attached to the substrate in rigor solution. The labeling pattern depended on sarcomere length. Relaxed skeletal myofibrils, with sarcomeres shorter than 2.5 μm, were labeled with TR-phalloidin with the same distribution as were rigor myofibrils (not shown). The thin filaments of relaxed skeletal myofibrils with sarcomere lengths longer than 3.1 μm were more uniformly stained than were rigor myofibrils of similar length (Fig.

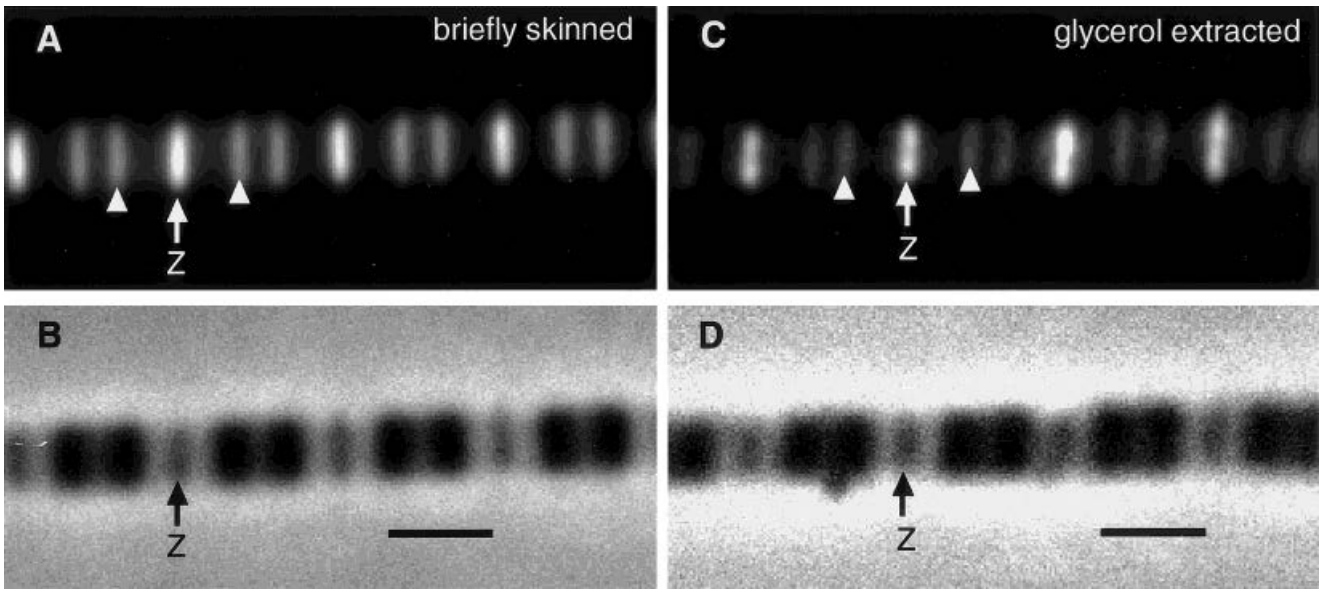

Fig. 1. Rhodamine-phalloidin staining of (**A,B**) short-term (16–18 h) skinned myofibrils and (**C,D**) long-term (7 day) glycerinated myofibrils: (A,C) total fluorescence and (B,D) corresponding phase contrast images. *Arrows* mark Z lines; *arrowheads* mark bright bands flanking the H zones. Scale bar = 2.0 μm.

3C). At intermediate sarcomere lengths, between 2.5 and 3.1 μm, groups of thin filaments in some sarcomeres labeled more uniformly; in other sarcomeres of the same myofibril, they were labeled nonuniformly as in rigor (Fig. 3A,B). For myofibrils with sarcomere length of 2.8–2.9 μm, 34% of the half sarcomeres were stained like rigor myofibrils, and for 3.1 μm, 17% were rigorlike. There was always a narrow (0.2 μm) weakly stained area on either side of the Z band in these stretched skeletal myofibrils (arrowheads in Fig. 3C).

Phalloidin binding to cardiac myofibrils was different from its binding to skeletal myofibrils (Fig. 3E). The fluorescence pattern in cardiac fibers, labeled while in rigor, contained a bright narrow band at the Z line (arrow in Fig. 4) and one (Fig. 4A) or two (Fig. 4C) bright broad bands between the Z lines. Adjacent to and on either side of the Z lines were narrow, 0.2-μm regions with lower fluorescence (arrowhead in Fig. 4A,C). The fluorescent pattern of relaxed cardiac (Fig. 3E) myofibrils was similar to the pattern in rigor cardiac myofibrils and in stretched, relaxed skeletal myofibrils.

The position of the phalloidin staining in skeletal muscle can be established from images of myofibrils at different sarcomere lengths. Figure 5 shows a single myofibril that contains sarcomeres with various lengths. Among the five sarcomeres shown, the sarcomere length changed, from left to right, from 1.7 μm to 2.5 μm. As the sarcomere length increases, the two fluorescent bands that flank the H zone (arrowheads in Fig. 5) appear to approach each other, merge, and then separate. Based on the structure of the sarcomeres, this behavior suggests that these two fluorescent bands correspond to the pointed ends of thin filaments. To quantify this effect, the gap between the two bands (filled squares in Fig. 6) and the distances from a Z line to either the nearer (open circles) or farther (filled circles) band were measured for a range of sarcomere lengths. The gap is zero for a sarcomere length of 2.15 μm. As the sarcomere length changes from 2.15 μm, the gap increases linearly, with a slope of approximately 1. For sarcomere lengths >2.15 μm, the separation of Z line and the nearer of the bands flanking the H zone is independent of sarcomere length and is approximately 1.1 μm, the length of a thin filament.

In cardiac cells, the broad band of phalloidin staining between the Z lines separated into two bands at longer sarcomere lengths (Fig. 4C). The separation between the centroids of the two bands depended linearly on sarcomere length (not shown). The widths of the separated broad fluorescent bands were about 0.8 μm independent of sarcomere length. The distance from the Z line to the farther edge of the bright region was about 1.0 μm, similar to the expected length of cardiac thin filaments.

Specificity of Phalloidin Binding

To test whether other fluorescently labeled proteins bind to Z lines or pointed ends of the thin filaments, bovine serum albumin labeled with succinimide rhodamine (SR-BSA) was added to briefly skinned myofibrils and fluorescent images acquired. The SR-BSA bound to

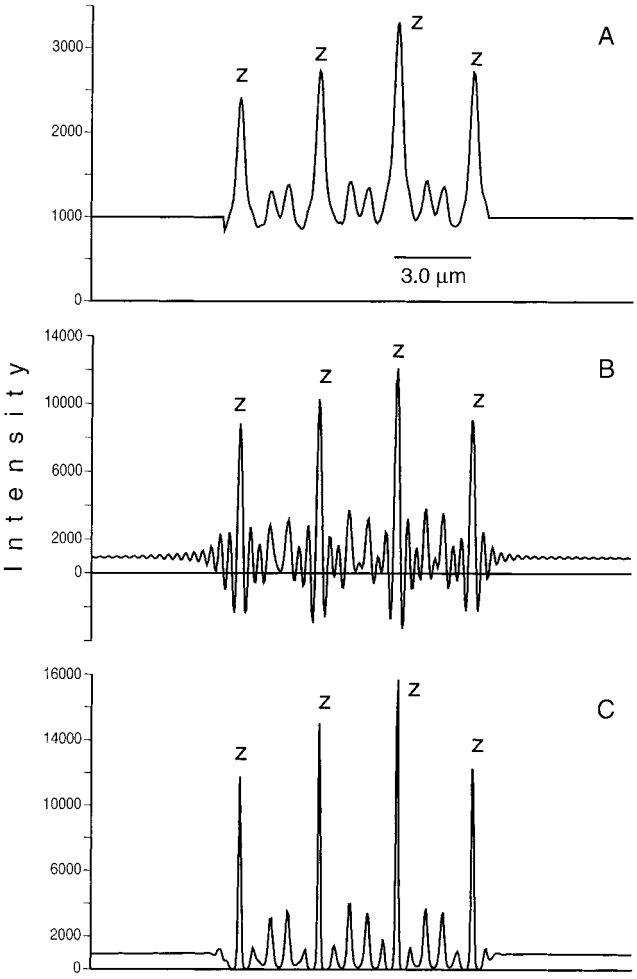

Fig. 2. Fluorescence intensity of rhodamine-phalloidin-labeled skeletal myofibril (**A**) projected along the long axis of the myofibril (**B**) after resolution enhancement using a Wiener filter deconvolution and (**C**) after maximum entropy deconvolution.

the fibers was uniform throughout the myofibril, lower than that bound to the coverslip and lower than phalloidin labeling of myofibrils (data not shown).

To determine whether the nonuniform labeling of the sarcomere was due to spatial variations in the number of TR-phalloidin binding sites or to multiple classes of binding sites, steady-state fluorescence polarization microscopy was used to measure the local orientation of rhodamine in the myofibril. Previous measurements on single bare actin filaments labeled with TR-phalloidin indicated that the fluorophore was oriented primarily along the axis of the F-actin [Prochniewicz-Nakayama et al., 1983; Kinoshita et al., 1991; Zhukarev et al., 1995]. Digitized images of briefly skinned myofibrils were acquired with four combinations of excitation and emission polarizer orientations (Fig. 7A–D) and were combined numerically to produce polarization ratio images, $P_{\parallel} = (\parallel I_{\parallel} - \parallel I_{\perp})/(\parallel I_{\parallel} + \parallel I_{\perp})$ (Fig. 7E) and $P_{\perp} = (_{\perp}I_{\perp} - _{\perp}I_{\parallel})/(_{\perp}I_{\perp} + _{\perp}I_{\parallel})$ (Fig. 7F). In both ratio images, three

TABLE I. Myofibrils Labeled in Mg-Rigor Solution

	Z lines	Pointed end of thin filaments	Remainder of thin filaments
Skeletal, briefly skinned (n = 6)			
label %	37.5 ± 3.6	42.6 ± 4.1	10.8 ± 3.8
$P_{\parallel}$ ± SEM	0.251 ± 0.011	0.269 ± 0.023	0.317 ± 0.023
$P_{\perp}$	0.064 ± 0.031	0.055 ± 0.034	0.008 ± 0.024
Skeletal, glycerol extracted (n = 4)			
label %	32.3 ± 14.8	48.3 ± 14.8	16.4 ± 3.4
$P_{\parallel}$	0.150 ± 0.019	0.156 ± 0.033	0.263 ± 0.023
$P_{\perp}$	0.180 ± 0.063	0.156 ± 0.036	0.046 ± 0.039
Cardiac, briefly skinned (n = 8)			
label %	12.4 ± 3.6		87.2 ± 3.8
$P_{\parallel}$	0.245 ± 0.015		0.268 ± 0.019
$P_{\perp}$	0.061 ± 0.030		0.003 ± 0.023

regions of rhodamine ordering are observed. Pseudo-color images combining the magnitude of the fluorescence intensity, coded as brightness, and polarization ratios, coded as hue, are shown in Figure 7E,F. At all points along the myofibril, the parallel ratio is larger than the perpendicular ratio; however, at the Z line (Z in Fig. 7A) and the pointed ends of the thin filaments (arrowheads in Fig. 7A), the difference between these polarization ratios is smaller than that in the thin filament region between the two ends. These data show that TR-phalloidin is bound with its transition dipole aligned primarily along the myofibril axis and that the TR-phalloidin is slightly more ordered in the middle than at the ends of the filaments. Pseudo-color polarization ratio images for cardiac myofibrils (Fig. 8) show that the TR-phalloidin fluorophores are also oriented along the fibril axis. The average polarization ratios (±SEM) of bound TR-phalloidin for the three regions of rigor skeletal and cardiac myofibrils are shown in Table I. At both the Z lines and the pointed ends of the thin filaments in glycerol-extracted myofibrils, $P_{\parallel}$ is nearly equal to $P_{\perp}$, suggesting that the phalloidin bound to the ends of these filaments is poorly ordered.

The fluorescence polarization ratios for relaxed myofibrils (Table II) were slightly different from those for rigor myofibrils (Table I) for both skeletal and cardiac muscle, suggesting lower ordering of relaxed thin filament actin in general. For both conditions, the probes were less ordered at the Z lines and at the pointed ends of the filaments than at the middle of thin filament. This difference was larger in glycerol-extracted than in briefly skinned myofibrils.

To test whether high-density binding and resultant ''self''-energy transfer or concentration depolarization [van der Meer et al., 1994] is responsible for lowering the fluoresence polarization at the ends of the thin filaments,

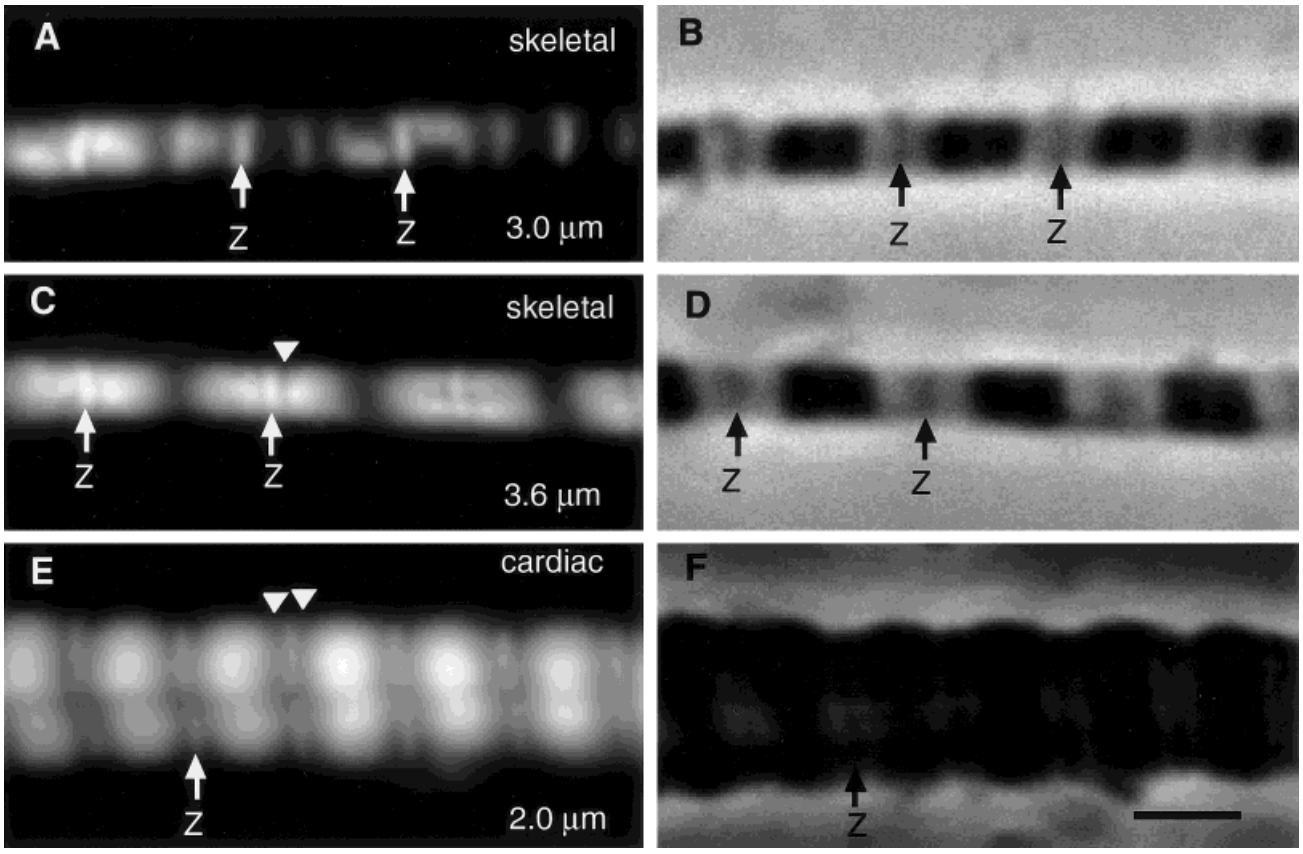

Fig. 3. Skeletal (**A–D**) and cardiac (**E,F**) myofibrils labeled in relaxing solution: (A,C,E) fluorescence and (B,D,F) phase contrast images. Skeletal myofibrils with 3.0 µm (A,B) and 3.6 µm (C,D) sarcomere lengths label differently. *Arrows* mark Z lines. Note the increased binding of the phalloidin in the relaxed skeletal myofibrils (A,C) and the small dark lines near the Z bands (A,C,E). Scale bar = 2.0 µm.

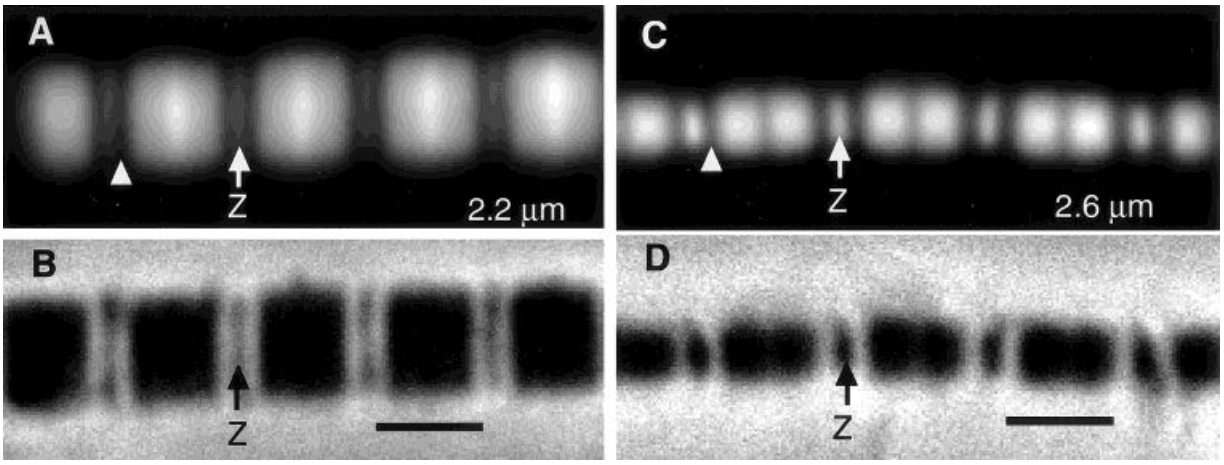

Fig. 4. The total fluorescence (**A,C**) and phase contrast (**B,D**) images of two cardiac myofibrils labeled in rigor solution: sarcomere length = 2.2 µm in A,B, and 2.6 µm in C,D. *Arrows* mark Z lines; *arrowheads* mark narrow regions with lower fluorescence adjacent to the Z lines. Scale bar = 2.0 µm.

skeletal myofibrils were stained with TR-phalloidin diluted with unlabeled phalloidin. Although the total average fluorescence intensity was lower in myofibrils stained with the diluted labeled phalloidin (17% of control for a 7:1 ratio of labeled:unlabeled phalloidin and 10% of control for a 3:1 ratio of labeled:unlabeled phalloidin), the polarization ratios and intensity distributions were unaffected.

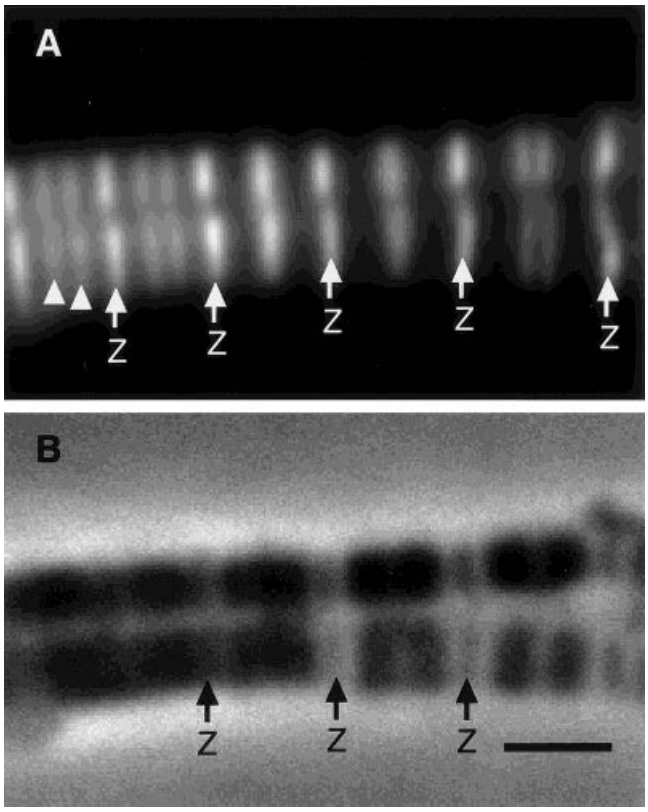

Fig. 5. Phalloidin-stained skeletal myofibril that contains sarcomeres with various lengths. **A** shows total fluorescence; **B** is a phase contrast image. In the five sarcomeres shown, the sarcomere length changes, from left to right, from 1.7 to 2.5 μm. *Arrows* mark Z lines; *arrowheads* mark bright bands flanking the H zones. Scale bar = 2.0 μm.

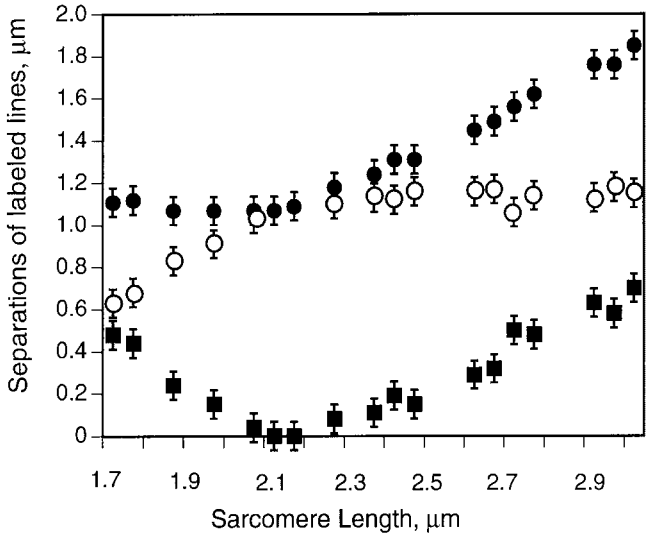

Fig. 6. The relative positions of the phalloidin-stained lines in skeletal myofibrils measured for a range of sarcomere lengths. Separation of the two bands flanking the H zone (*filled squares*), distance between the Z line and the farther of the bands flanking the H zone (*filled circles*), and distance between the Z line and the nearer of the bands flanking the H zone (*open circles*). (Means ± SD for three sarcomeres).

Do Sarcomeric Proteins Block Phalloidin Binding?

To study whether myosin, tropomyosin, or troponin block the binding of TR-phalloidin in skeletal myofibrils, thick filaments were extracted in a high-ionic-strength buffer. The resultant ghost myofibrils were then stained with TR-phalloidin while in rigor solution (Fig. 9A,B). The Z lines (large arrows in Fig. 9A,B) are brightly stained, as are structures 1.1 μm from the Z lines (arrowheads in Fig. 9A). Occasionally, myofibrils were found with skewed Z lines (small arrows in Fig. 9A). The Z lines and the flanking lines, 1.1 μm from their respective Z lines, remained parallel even in skewed sarcomeres. These data further support the hypothesis that the bright bands flanking the H zone are the pointed ends of thin filaments. The phalloidin staining pattern of ghost myofibrils was the same whether they were in rigor or relaxing solution when labeled with phalloidin (not shown). These results corroborate previous studies [Szczesna and Lehrer, 1993] that show that the removal of myosin together with the tropomyosin–troponin complex does not affect phalloidin binding.

To determine whether the removal of the tropomyosin–troponin complex separately from myosin changes the binding of TR-phalloidin to the thin filaments, myofibrils were exposed to a 1.0-mM sodium bicarbonate, pH 8.0 solution, previously shown to extract these proteins [Sanger et al., 1984]. The supernatant from the bicarbonate treatment was run on gels and, as previously reported, showed bands with the mobility of tropomyosin and the troponins (data not shown), indicating at least partial extraction. The phalloidin staining of extracted skeletal myofibrils was identical to that in unextracted myofibrils. Thus, the nonuniformity of thin filament staining by TR-phalloidin is not likely due to blocking by either myosin or the tropomyosin–troponin complex.

α-Actinin added to isolated myofibrils binds to Z lines and enables new actin filaments to polymerize from the Z lines after adding monomer actin [Sanger et al. 1984]. TR-phalloidin bound uniformly to newly formed actin filaments for ~1 μm on either side of the Z line (arrows in Fig. 10A), with a small decrease in intensity at the M line (arrowheads in Fig. 10A) of each sarcomere. The fluorescence polarization ratios measured in these myofibrils were $P_{\|} = 0.296 \pm 0.025$ and $P_{\perp} = -0.014 \pm 0.034$ and were uniform throughout the sarcomere, implying consistantly higher ordering than that found in the endogenous thin filaments (Fig. 10C,D). When monomer actin was added to myofibrils without the prior addition of α-actinin, new actin filaments formed only in the A band, as shown previously [Sanger et al., 1984].

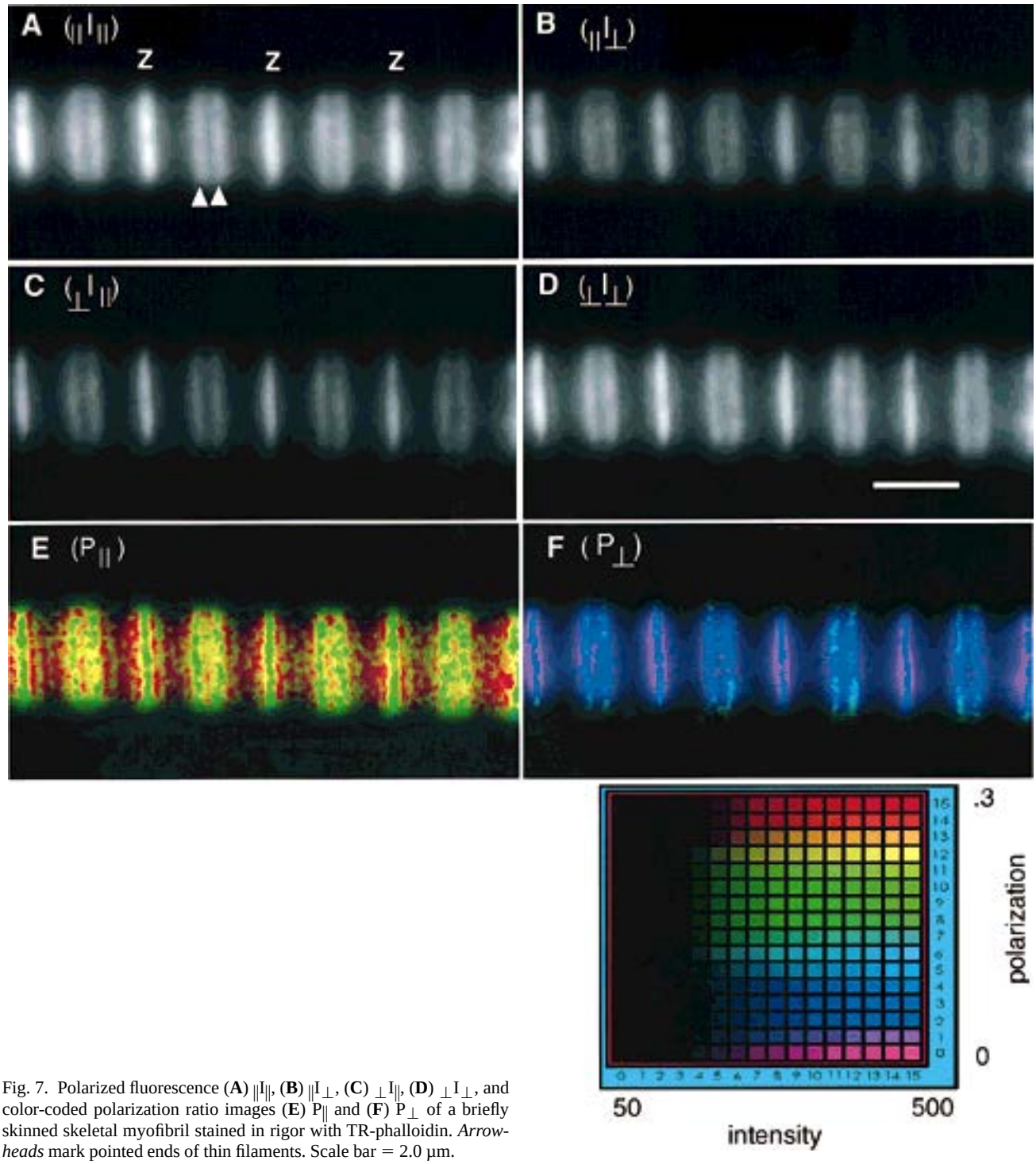

Fig. 7. Polarized fluorescence (**A**) $_{\parallel}I_{\parallel}$, (**B**) $_{\parallel}I_{\perp}$, (**C**) $_{\perp}I_{\parallel}$, (**D**) $_{\perp}I_{\perp}$, and color-coded polarization ratio images (**E**) $P_{\parallel}$ and (**F**) $P_{\perp}$ of a briefly skinned skeletal myofibril stained in rigor with TR-phalloidin. *Arrowheads* mark pointed ends of thin filaments. Scale bar = 2.0 μm.

The TR-phalloidin staining of these new filaments was also uniform.

DISCUSSION

We have confirmed several previous reports that TR-phalloidin binds more intensely at the Z line and in two bright bands flanking the H zone of skeletal muscle. The bands flanking the H zone were consistent with phalloidin binding at the pointed ends of thin filaments. The thin filaments of cardiac myofibrils had previously been shown to label uniformly with phalloidin [Ao and Lehrer, 1995], but, contrary to those results, the data reported in the present study show that there are narrow

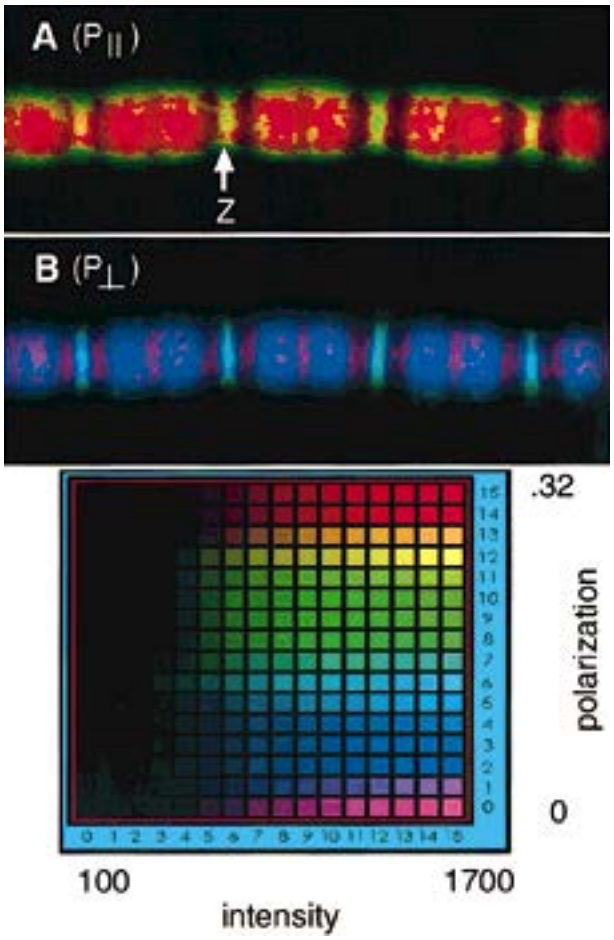

Fig. 8. Color coded polarization ratio images, $P_{\parallel}$ (**A**) and $P_{\perp}$ (**B**), for the cardiac myofibril shown in Figure 4C,D.

(~0.2 μm) bands adjacent to the Z lines of cardiac cells that have weaker phalloidin labeling than the remainder of the thin filaments. Ao and Lehrer [1995] also found that long-term (3 h) staining with phalloidin at room temperature changed the fluorescent labeling distribution in cardiac cells, whereas we found no change between short- and long-term staining at 4°C. The difference could be that long-term staining at room temperature leads to significant degradation of sarcomeric proteins, whereas incubation on ice does not lead to degradation, although other experimental differences such as the muscle type, the phalloidin, or the detection conditions used could account for the different observations.

Our data imply that there is either inhibition of phalloidin binding at the middle of the thin filament with respect to the two ends or an excess of nonspecific binding sites at both ends of the filament. The indirect evidence suggests that the phalloidin binding sites are blocked in the middle of the thin filaments in skeletal muscle. First, labeled albumin, expected to bind to nonspecific sites in the myofibril, binds uniformly along

TABLE II. Myofibrils Labeled in 15 mM ATP Relaxing Solution

	Z lines	Pointed end of thin filaments	Remainder of thin filaments
Skeletal, briefly skinned without tips (n = 7)			
label %	32.6 ± 9.7		55.3 ± 4.0
$P_{\parallel}$ ± SEM	0.253 ± 0.022		0.293 ± 0.014
$P_{\perp}$	0.048 ± 0.022		0.015 ± 0.031
With tips (n = 4)			
label %	37.2 ± 6.4	36.5 ± 1.4	23.7 ± 4.0
$P_{\parallel}$	0.263 ± 0.010	0.284 ± 0.003	0.298± 0.003
$P_{\perp}$	0.033 ± 0.015	0.007 ± 0.003	0.000 ± 0.005
Skeletal, glycerol extracted (n = 6)			
label %	36.1 ± 3.9	29.9 ± 4.2	32.3 ± 4.7
$P_{\parallel}$	0.169 ± 0.019	0.206 ± 0.033	0.226 ± 0.010
$P_{\perp}$	0.199 ± 0.036	0.165 ± 0.035	0.144 ± 0.036
Cardiac, briefly skinned (n = 8)			
label %	37.0 ± 4.9		60.3 ± 5.8
$P_{\parallel}$	0.262 ± 0.010		0.266 ± 0.010
$P_{\perp}$	0.034 ± 0.012		−0.018 ± 0.006

the sarcomere, suggesting that there is not an excess of nonspecific sites at the Z line or pointed ends of the thin filaments. Second, actin, in relaxed myofibrils stretched to long sarcomere lengths, label uniformly and with the same brightness as the Z line and tips (Fig. 3). Third, myofibrils incorporating newly polymerized, bare actin filaments appear to be far more brightly stained with TR-phalloidin than do the middles of the endogenous filaments, virtually eliminating contrast along the sarcomeres (Fig. 10).

Whereas the binding and polymerization studies have suggested that phalloidin binding is inhibited in the middle of the thin filaments, the fluorescence polarization evidence is not as clear. Fluorescence polarization microscopy is a sensitive method for measuring local molecular orientation [Axelrod, 1979; Zhukarev et al., 1995]. Phalloidin bound specifically to straight filaments should result in uniform orientation of the molecule and of its bound fluorophor, whereas phalloidin bound nonspecifically to disordered filaments is expected to result in fluorophors with angular disorder. To test whether the specificity of phalloidin binding to actin differs along muscle filaments and whether phalloidin binds to thin filaments in myofibrils the same way as it binds to actin filaments, fluorescence polarization of rhodamine phalloidin was measured microscopically in two muscle types and in two preparations of F-actin polymerized within myofibrils. In cardiac and briefly skinned myofibrils, the polarization ratios of bound phalloidin are nearly the same all along the thin filament, implying that the

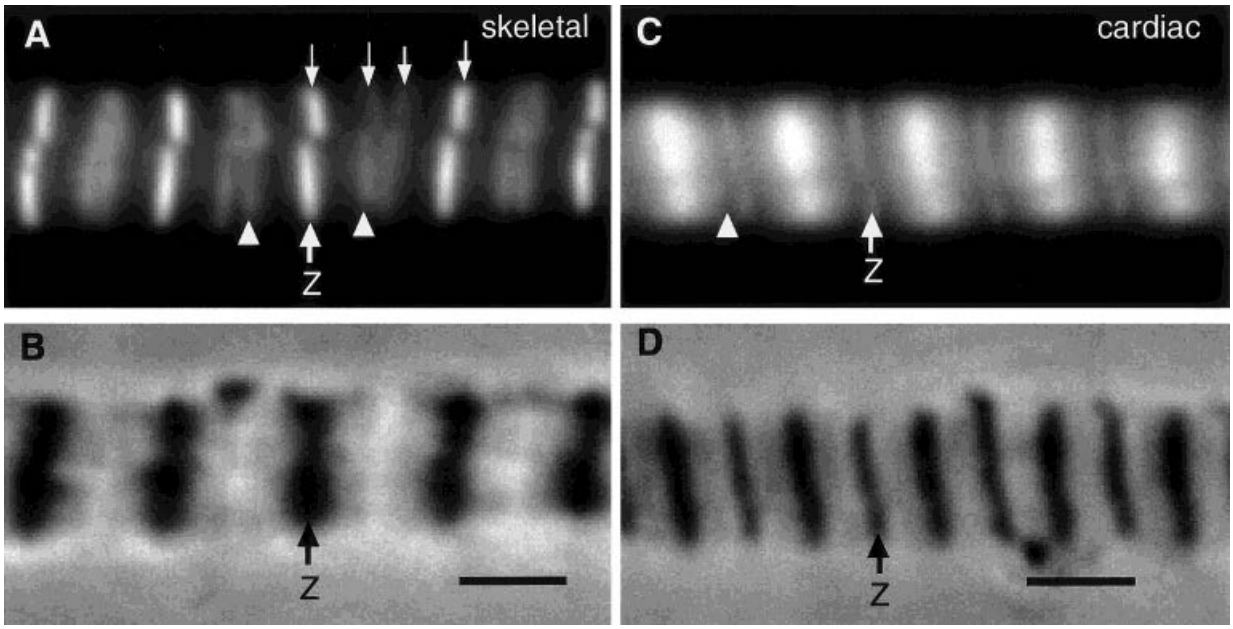

Fig. 9. Myosin has been extracted from these myofibrils, leaving behind ghost myofibrils. Phalloidin-stained ghost myofibrils from skeletal (**A,B**) and cardiac (**C,D**) myofibrils: (A,C) fluorescence and (B,D) phase contrast images. A skewed sarcomere is visible in A (*small arrows*). *Large arrows* mark Z lines; *arrowheads* mark bright bands flanking the H zones. Scale bar = 2.0 μm.

orientation of phalloidin is also uniform. All of the fluorophores appear to be oriented predominantly along the long axis of the myofibrils in the sarcomere, suggesting that the phalloidin binding sites are similar at the ends and middle of the filament. However, the parallel excitation ratios, $P_{\parallel}$, and the perpendicular excitation ratios, $P_{\perp}$, at the ends of the thin filaments are closer in value than they are in the middle of the filament in both muscle types, suggesting the dye is slightly less well ordered at the ends of the filaments. In addition, we found that phalloidin binds with higher order to newly polymerized exogenous actin than it does to endogenous actin, suggesting that the phalloidin binding site is different in F-actin and the endogenous thin filaments. The newly polymerized actin filaments do not have any other proteins bound to them (no nebulin, tropomyosin, or troponins) and thus may bind rhodamine phalloidin differently than native thin filaments.

In glycerol-extracted skeletal muscle, $P_{\parallel} \approx P_{\perp}$ at the Z line and pointed ends of the thin filaments, indicating that the dye is either bound to the ends of thin filaments at the magic angle (54.7°) to the fibril axis or with random orientation. This possibility suggests that long-term glycerination changes the structure of the thin filaments so that either (1) the binding is nonspecific at these sites and the orientation of the dye in the Z lines and the pointed ends of the thin filaments does not reflect the orientation of the thin filaments themselves or (2) the ends of the thin filaments have disordered orientations. Because it is difficult to determine the orientations of the ends of the actin filaments in glycerinated myofibrils from electron microscope images [Huxley, 1957], we cannot yet distinguish these two possibilities.

Phalloidin binding to the middle of the thin filaments in skeletal muscles might be blocked by other muscle proteins such as myosin, tropomyosin, nebulin, or titin. The bicarbonate and high salt extraction experiments on isolated myofibrils suggest, as found previously [Szczesna and Lehrer, 1993], that neither myosin nor the tropomyosin–troponin complex inhibits TR-phalloidin binding to the thin filaments. Cardiac and skeletal myofibrils bind phalloidin differently, but both have titin, suggesting that titin is not responsible for inhibiting phalloidin binding. The correlation of a shorter nebulin molecule, i.e., nebulette, with a narrower band of low phalloidin binding in cardiac muscle suggests that nebulin isoforms are responsible for the blockage of TR-phalloidin binding in myofibrils. The difference in the size of skeletal nebulin (molecular weight 800 kD) and the cardiac homologue, nebulette (molecular weight 107 kD) [Moncman and Wang, 1995] is consistent with skeletal muscle nebulin blocking phalloidin binding along a larger portion of the thin filament and with cardiac muscle nebulette blocking only a short section of the filament adjacent to the Z line. This interpretation is supported by the observation that the 35-mer repeat fragment of nebulin binds to the central cleft of the actin

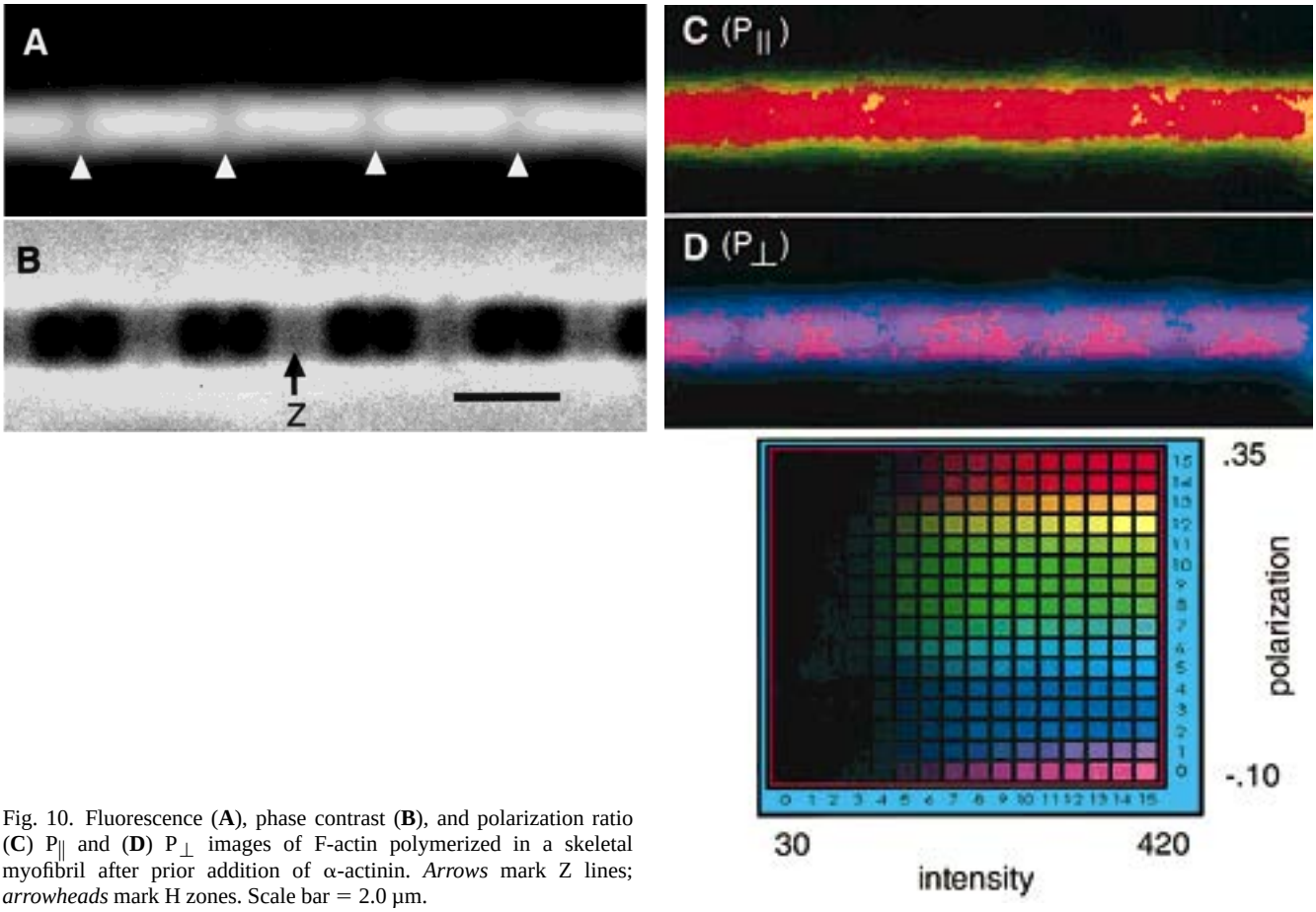

Fig. 10. Fluorescence (**A**), phase contrast (**B**), and polarization ratio (**C**) $P_{\|}$ and (**D**) $P_{\perp}$ images of F-actin polymerized in a skeletal myofibril after prior addition of α-actinin. *Arrows* mark Z lines; *arrowheads* mark H zones. Scale bar = 2.0 μm.

polymer, which is also the site for the binding of phalloidin to F-actin [Pfuhl et al., 1994].

Our data imply that the state of the cross bridges changes TR-phalloidin binding to thin filaments in briefly skinned fibers, at long sarcomere lengths, and in glycerinated fibers at all sarcomere lengths. The difference between TR-phalloidin binding to glycerinated myofibrils and to briefly skinned myofibrils is more pronounced in relaxed myofibrils (Table II). An explanation may be that glycerination removes some structural proteins (tropomyosin–troponin, nebulin, or titin) from the thin filament, thereby making the filaments less straight. The rigor cross bridges may straighten the filaments, but after relaxation the filaments are slack and wavy, which would lead to a smaller difference between the $P_{\|}$ and $P_{\perp}$ fluorescence polarization ratios. Some support for this extraction interpretation is given by data on the exposure of myofibrils to the actin-severing protein gelsolin [Funatsu et al., 1990; Gonsior and Hinssen 1995]. If myofibrils, previously stored in glycerol, were exposed to gelsolin, thin filaments were extracted from the sarcomeres [Funatsu et al., 1990]. In contrast, if skeletal myofibrils, freshly isolated and permeabilized using detergent, were exposed to gelsolin, thin filaments were not extracted [Gonsior and Hinssen 1995]. In freshly isolated cardiac myofibrils, gelsolin treatment resulted in thin filament extraction, leading to the suggestion that nebulin is responsible for the gelsolin resistance of freshly isolated skeletal myofibrils and that prolonged glycerination might cause extraction of nebulin [Gonsior and Hinssen 1995]. Structural changes due to glycerol extraction also have been observed with electron microscopy of fixed muscle [Huxley, 1957].

An explanation for the dependence of TR-phalloidin binding on the sarcomere length (Fig. 3) in briefly skinned myofibrils is far more speculative. We hypothesize that stretching a sarcomere leads to the displacement of nebulin from F-actin. Titin has been hypothesized to be the muscle component that senses a change in the sarcomere length [Horowits et al., 1986]. When muscle is stretched, the structure of titin is changed [Furst et al., 1988; Itoh et al., 1988]. A possible mechanism for the displacement of nebulin is an interaction of titin with nebulin or with F-actin. The elongation of titin could then either directly perturb nebulin or change the thin filament structure so that nebulin is no longer as tightly bound,

which would allow the increased binding of phalloidin to actin.

SUMMARY

Phalloidin is used widely to localize and quantify the amount of F-actin in cells. It has also been used to measure the orientation distribution of F-actin in composite actin structures and to monitor orientation or structural changes in thin filaments during muscle contraction. The results presented in this article suggest that phalloidin-based probes are not a reliable monitor for all of the F-actin in all cell types and should be used with caution to quantitate the amount and organization of actin in cardiac and skeletal muscle cells. The detailed behavior of phalloidin binding with changes in sarcomere length and biochemical state of the cross bridges suggests length-sensing mechanisms within the sarcomere that influence actin at its phalloidin binding site.

ACKNOWLEDGMENTS

This work was supported by a grant from the NIH (HL-15835 to the Pennsylvania Muscle Institute; HL-48954 to J.W.S.) and NSF (MCB-93-19041 to J.M.S.).

REFERENCES

Allen, T.S., Ling, N., Irving, M., and Goldman, Y.E. (1996): Orientation changes in myosin regulatory light chains following photorelease of ATP in skinned muscle fibers. Biophys. J. 70:1847–1862.

Ao, X., and Lehrer, S.S. (1995): Phalloidin unzips nebulin from thin filaments in skeletal myofibrils. J. Cell Sci. 108:3397–3403.

Axelrod, D. (1979): Carbocyanine dye orientation in red cell membrane studied by microscopic fluorescence polarization. Biophys. J. 26:557–574.

Borejdo, J., and Burlacu, S. (1993): Measuring orientation of actin filaments within a cell: Orientation of actin in intestinal microvilli. Biophys. J. 65:300–309.

Bukatina, A.E., Sonkin, B.Y., Alievskaya, L.L., and Yashin, V.A. (1984): Sarcomere structures in the rabbit psoas muscle as revealed by fluorescent analogs of phalloidin. Histochemistry 81:301–304.

Danowski, B.A., Imanaka-Yoshida, K., Sanger, J.M., and Sanger, J.W. (1992): Costameres are sites of force transmission to the substratum in adult rat cardiomyocytes. J. Cell Biol. 118:1411–1420

Faulstich, H., Zobeley, S., Rinnerthaler, G., and Small, J.V. (1988): Fluorescent phallotoxins as probes for filamentous actin. J. Mus. Res. Cell Motil. 9:370–383.

Fishkind, D.J., and Wang, Y. (1993): Orientation and three-dimensional organizational organization of actin filaments in dividing culture cells. J. Cell Biol. 123:837–848.

Funatsu, T., Higuchi, H., and Ishiwata, S. (1990): Elastic filaments in skeletal muscle revealed by selective removal of thin filaments with plasma gelsolin. J. Cell Biol. 110:53–62.

Furst, D.O., Osborn, M., Nave, R., and Weber, K. (1988): The organization of titin filaments in the half-sarcomere revealed by monoclonal antibodies in immunoelectron microscopy: A map of ten nonrepetitive epitopes starting at the Z line extends close to the M line. J. Cell Biol. 106:1563–1572.

Goldman, Y.E., Hibberd, M.G., and Trentham, D.R. (1984): Relaxation of rabbit psoas muscle fibres from rigor by photochemical generation of adenosine-triphosphate. J. Physiol. 354:577–604.

Gonsior, S., and Hinssen, H. (1995): Exogenous gelsolin binds to sarcomeric thin filaments without severing. Cell Motil. Cytoskeleton 31:196–206.

Horowits R., Kempner, E.S., Bisher, M.E., and Podolsky, R.J. (1986): A physiological role for titin and nebulin in skeletal muscle. Nature 323:160–164.

Huxley, H.E. (1957): The double array of filaments in cross-striated muscle. J. Biophys. Biochem. Cytol. 3:631–647.

Itoh, Y., Suzuki, T., Kimura, S., Ohashi, K., Higuchi, H., Sawada, H., Shimizu, T., Shibata, M., and Maruyama, K. (1988): Extensible and less-extensible domains of connectin filaments in stretched vertebrate skeletal muscle sarcomeres as detected by immunofluorescence and immunoelectron microscopy using monoclonal antibodies. J. Biochem. 104:504–508.

Kinoshita, K., Itoh, H., Ishiwata, S., Hirano, K., Nishizaka, K., and Hayakawa, T. (1991): Dual-view microscopy with a single camera: Real-time imaging of molecule orientations and calcium. J. Cell Biol. 115:67–73.

Kishino, A., and Yanagida, T. (1988): Force measurements by micromanipulation of a single actin filament by glass needles. Nature 334:74–76.

Kuzuo, R., and Tanaka, M. (1993): Resolution enhancement of electron-energy-loss spectra using the maximum-entropy method. J. Electron Microsc. 42:240–243.

Larsson, L., and Moss, R.L. (1993): Maximum velocity of shortening in relation to myosin isoform composition in single fibres from human skeletal muscles. J. Physiol. 472:595–614.

Locker, R.H., and Wild, D.J.C. (1986): A comparative study of high molecular weight proteins in various types of muscle across the animal kingdom. J. Biochem. (Tokyo) 99:1473–1484.

Lorenz M., Popp, D., and Holmes, K.C. (1993): Refinement of the F-actin model against X-ray fiber diffraction data by the use of a directed mutation algorithm. J. Mol. Biol. 234:826–36.

Moncman, C.L., and Wang, K. (1995): Nebulette: A 107 kD nebulin-like protein in cardiac muscle. Cell Motil. Cytoskeleton 32:205–225.

Pfuhl, M., Winder, S.J., and Pastore, A. (1994): Nebulin, a helical actin binding protein. EMBO J. 13:1792–1789.

Press, W.H., Flannery, B.P., Teukolsky, S.A., and Vetterling, W.T. (1988): ''Numerical Recipes in C.'' Cambridge, U.K. Cambridge University Press, pp. 434–437.

Prochniewicz-Nakayama, E., Yanagida, T., and Oosawa, F. (1983): Studies of F-actin in muscle fibers in the relaxed state, rigor, and during contraction using fluorescent phalloidin. J. Cell Biol. 97:1663–1667.

Sanger, J.W., Mittal, B., and Sanger, J.M. (1984): Analysis of myofibrillar structure and assembly using fluorescently labeled contractile proteins. J. Cell Biol. 98:825–833.

Szczesna, D., and Lehrer, S.S. (1993): The binding of fluorescent phallotoxins to actin in myofibrils. J. Mus. Res. Cell Motil. 14:594–597.

Tsien, R.Y., and Harootunian, A.T. (1990): Practical design criteria for a dynamic ratio imaging system. Cell Calcium 11:93–109.

van der Meer, B.W., Coker, G. III, and Chen, S.-Y. (1994): ''Resonance Energy Transfer: Theory and Data.'' New York, VCH Publishers.

Wang, K. (1984): Cytoskeletal matrix in striated muscle: The role of titin, nebulin and intermediate filaments. Adv. Exp. Med. Biol. 170:285–305.

Wehland J., Osborn, M., and Weber, K. (1977) Phalloidin-induced actin polymerization in the cytoplasm of cultured cells interferes with cell locomotion and growth. Proc. Natl. Acad. Sci. USA 74:5613–5617.

Wilson, P., Fuller, E., and Forer, A. (1987): Irradiations of rabbit myofibrils with an ultraviolet microbeam. II. Phalloidin protects actin in solution but not in myofibrils from depolymerization by ultraviolet light. Biochem. Cell Biol. 65:376–385.

Zhukarev, V., Ashton, F.T., Sanger, J.M., Sanger, J.W., and Shuman, H. (1995): Steady state fluorescence polarization study of actin filament bundles in Listeria-infected cells. Cell Motil. Cytoskeleton 30:229–246.

Zhukarev, V., Sanger, J.M., Sanger, J.W., Goldman, Y.E., and Shuman, H. (1996a): Fluorescence polarization microscopy of nonuniform phalloidin staining of myofibrils. Mol. Biol. Cell 7:537a.

Zhukarev, V., Sanger, J.M., Sanger, J.W., Goldman, Y.E., and Shuman, H. (1996b): Steady-state fluorescence polarization analysis of rhodamine-phalloidin binding to muscle. Biophys. J. 70:A268.

APPENDIX

Images of fluorescent objects are corrupted by the light microscope in two principal ways. First, the spatial resolution of the microscope is limited by diffraction and degraded further by imperfections in the lenses. Second, the measured image contains added noise, e(x,y). The noise can be due to excitation light passing through the dichroic mirror and emission filter, fluorescent light scattered in the microscope, or dark signal in the recording device. The effect that the microscope has on image resolution is called the point spread function, psf(x,y). The psf can be measured directly from images of objects smaller than the resolution limit of the microscope. The average microscope image, m(x,y), of a fluorescent object is the convolution of the fluorescent dye distribution, f(x,y), and the psf is

$$m(x, y) = psf(x, y) * f(x, y) = \int\int f(u, v)\, psf(x - u, y - v)\, du\, dv \quad (1)$$

where * indicates a convolution. The actual detected image, d(x,y), is the average microscope image, with added noise

$$d(x, y) = m(x, y) + e(x, y) = psf(x, y) * f(x, y) + e(x, y) \quad (2)$$

To simplify data analysis, the intensities of the two-dimensional images of the fibrils are averaged in the y direction, perpendicular to fibril axis:

$$d'(x) = \int d(x, y)\, dy = \iiint f(u, v)\, psf(x - u, y - v)\, du\, dv\, dy + \int e(x, y)\, dy$$

$$d'(x) = psf'(x) * f'(x) + e'(x) \quad (3)$$

where the primes indicate the one-dimensional images

$$psf'(x) = \int psf(x, y)\, dy,\ f'(x) = \int f(x, y)\, dy \text{ and } e'(x) = \int e(x, y)\, dy$$

For numerical calculations, equation (3) is digitized to

$$d_i = \Sigma_k\ psf_{i-k}\, f_k + e_k \quad (4)$$

where the indices i and k range over N discrete pixels and psf_i, f_i, and e_i are the digitized psf, dye distribution, and noise, respectively. For simplicity, the resolution of the microscope was assumed to be limited entirely by diffraction and the two-dimensional psf assumed to be an Airy function

$$psf(x, y) = J_1^2(kr)/(kr)^2$$

where $r^2 = x^2 + y^2$ and J_1 is the first-order Bessel function. The one-dimensional psf is then

$$psf(x) = \int J_1^2(kr)/(kr)^2\, dy.$$

The resolution parameter k was determined by fitting psf(x) to fluorescence images of phalloidin-stained single actin filaments. In our microscope, $k = 0.0136\ nm^{-1}$.

Wiener Filter

The discrete Fourier transform of equation (4) is

$$D_j = PSF_jF_j + E_j$$

where D_j, PSF_j, F_j, and E_j are the transforms of d_i, psf_i, f_i, and e_i, respectively. In the absence of noise, the Fourier transform of the true image F would be given by

$$F_j = D_j/PSF_j$$

but in the presence of noise, division by the smallest values in PSF_j would lead to an image dominated by high spatial frequency noise. The optimal filter [Press et al., 1988] to suppress the high spatial frequency noise is the Wiener filter:

$$F_j = D_jW_j/PSF_j, \text{ where}$$

$$W_j = |PSF_jF_j|^2/(|PSF_jF_j|^2 + |E_j|^2). \quad (5)$$

Because F is unknown, it is assumed that

$$|PSF_jF_j|^2 + |E_j|^2 \cong |D_j|^2.$$

At spatial frequencies higher than an estimated j_{cutoff}, the noise dominates the signal

$$|E_j|^2. \cong |D_j|^2, \text{ for } j > j_{cutoff}.$$

The high frequency noise can be extrapolated (ext) back to lower spatial frequencies; in particular, if the noise

amplitude is independent of frequency (white noise), it is

$$|E_j|^2(\text{ext})(j < j_{\text{cutoff}}) = |E_j|^2(j > j_{\text{cutoff}}) \text{ so that}$$
$$|PSF_jF_j|^2 = |D_j|^2 - \|D_j|^2(j > j_{\text{cutoff}}), \text{ and}$$
$$W_j = |D_j|^2 - |D_j|^2(j > j_{\text{cutoff}})/|D_j|^2. \quad (6)$$

The Wiener filter computed from equation (6) is is then substituted into equation (5) and used to calculate F, the Fourier transform of the corrected image. To obtain the image, f, the inverse transform, is performed on F. A typical result is shown in Figure 2B.

Iterative Maximum Entropy Deconvolution

Following Kuzuo and Tanaka [1993], the constrained entropy, S, of the image given by equation (4) is defined to be

$$S = -\Sigma_i f_i \log (f_i/f_{i0}) - \lambda Q(f) \text{ where}$$
$$Q(f) = \Sigma_i(d_i - \Sigma_k \, psf_{i-k} \, f_k)^2/\sigma_i^2,$$

where f_{io} is the prior image, λ is a Lagrange multiplier, and σ_i is the estimated variance at the i^{th} pixel of the image noise e_i. After maximizing S with respect to f_i, an iterative equation for f_i is found [Kuzuo and Tanaka, 1993]:

$$f_j^{(k+1)} = f_j^{(k)} \exp (-1 - \lambda Q_j[f^{(k)}]) \quad (7)$$

where $Q_j[f]$ is the partial derivative of Q with respect to f_i,

$$Q_j[f] = \delta Q_j[f]/\delta f_j = \Sigma_i \{psf_{i-j}(\Sigma_k \, psf_{i-k} \, f_k - d_i)/\sigma_i^2\}$$

and f is normalized after each iteration so that

$$\Sigma f_j^{(k+1)} = \Sigma \, d_j.$$

The maximum entropy image, f_j, that best fits the data for the unconstained case, $\lambda = 0$, can be found analytically to be

$$f_j = \Sigma \, d_j/N,$$

a uniform, flat image with the same average intensity as the original image. For all of the data discussed in the Appendix, the uniform image was chosen as the starting point for the iteration, so that

$$f_j^{(0)} = \Sigma \, d_j/N \ldots f_j^{(1)} = f_j^{(0)} \exp (-1 - \lambda Q_j[f^{(0)}]) \ldots \text{etc.}$$

The iteration was continued until the ratio $\Sigma_i (d_i - \Sigma_k \, psf_{i-k} \, f_k)^2/\Sigma_i \, d_i^2$ was smaller than 4×10^{-6}. The value of the Lagrange multipier λ, in the iteration equation (7), changes the rate of convergence of the iteration if λ is chosen to be too small, the chi-square statistic, Q(f), decreases slowly, and the convergence is slow. If λ is chosen to be too large, the iteration becomes unstable. The optimum value of λ was found by increasing λ at each step of the iteration until Q(f) began to increase, at which point λ was reduced and the iteration continued. Experimentally, the optimum λ scaled inversely, $\lambda_{opt} \sim 1/\sigma^2$, with the noise in the images.

Because $(-1 - \lambda Q_j[f^{(k)}])$ is always real and each pixel intensity in the initial guess is positive, each pixel in the new image at each step of the iteration is also positive. This positive definite constraint, in addition to the smoothing property of the maximum entropy method, leads to deconvoluted images (Fig. 2C) that appear to have lower ripple than the images deconvoluted with the Wiener filter (Fig. 2B).